



**HAL**  
open science

# Unexpected rapid aerobic transformation of 2,2,6,6-tetraethyl-4-oxo (piperidin-1-yloxy) radical by cytochrome P450 in the presence of NADPH: Evidence against a simple reduction of the nitroxide moiety to the hydroxylamine

Nikola Babić, Maylis Orio, Fabienne Peyrot

## ► To cite this version:

Nikola Babić, Maylis Orio, Fabienne Peyrot. Unexpected rapid aerobic transformation of 2,2,6,6-tetraethyl-4-oxo (piperidin-1-yloxy) radical by cytochrome P450 in the presence of NADPH: Evidence against a simple reduction of the nitroxide moiety to the hydroxylamine. *Free Radical Biology and Medicine*, 2020, 156, pp.144-156. 10.1016/j.freeradbiomed.2020.05.021 . hal-02895031

**HAL Id: hal-02895031**

**<https://hal.science/hal-02895031>**

Submitted on 10 Jul 2020

**HAL** is a multi-disciplinary open access archive for the deposit and dissemination of scientific research documents, whether they are published or not. The documents may come from teaching and research institutions in France or abroad, or from public or private research centers.

L'archive ouverte pluridisciplinaire **HAL**, est destinée au dépôt et à la diffusion de documents scientifiques de niveau recherche, publiés ou non, émanant des établissements d'enseignement et de recherche français ou étrangers, des laboratoires publics ou privés.

## Unexpected rapid aerobic transformation of 2,2,6,6-tetraethyl-4-oxo(piperidin-1-yloxy) radical by cytochrome P450 in the presence of NADPH: evidence against a simple reduction of the nitroxide moiety to the hydroxylamine.

**Authors:** Nikola Babić<sup>1</sup>, Maylis Orio<sup>2</sup>, and Fabienne Peyrot<sup>1,3,\*</sup>

### Affiliations:

<sup>1</sup> Université de Paris, Laboratoire de Chimie et Biochimie Pharmacologiques et Toxicologiques, UMR 8601, CNRS, F-75006 Paris, France

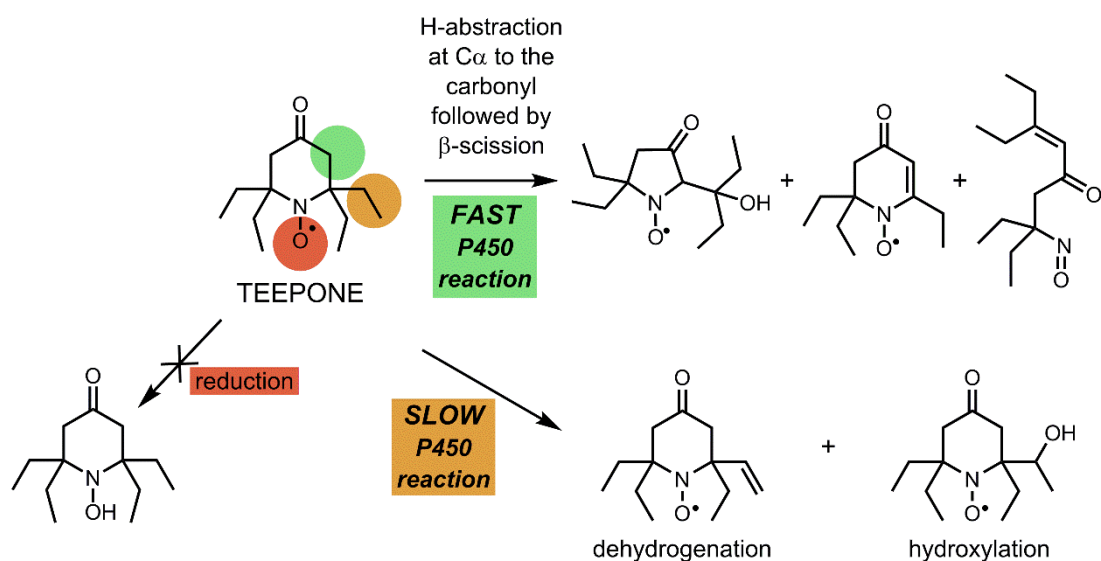
<sup>2</sup> Aix-Marseille Univ., CNRS, Centrale Marseille, iSm2, Marseille, France

<sup>3</sup> Sorbonne Université, Institut National Supérieur du Professorat et de l'Éducation (INSPE) de l'Académie de Paris, F-75016 Paris, France

\* **Correspondence:** fabienne.peyrot@u-paris.fr

### Abstract:

Aminoxyl radicals (nitroxides) are a class of compounds with important biomedical applications, serving as antioxidants, spin labels for proteins, spin probes of oximetry, pH, or redox status in electron paramagnetic resonance (EPR), or as contrast agents in magnetic resonance imaging (MRI). However, the fast reduction of the radical moiety in common tetramethyl-substituted cyclic nitroxides within cells, yielding diamagnetic hydroxylamines, limits their use in spectroscopic and imaging studies. In vivo half-lives of commonly used tetramethyl-substituted nitroxides span no more than a few minutes. Therefore, synthetic efforts have focused on enhancing the nitroxide stability towards reduction by varying the electronic and steric environment of the radical. Tetraethyl-substitution at alpha position to the aminoxyl function proved efficient in vitro against reduction by ascorbate or cytosolic extracts. Moreover, 2,2,6,6-tetraethyl-4-oxo(piperidin-1-yloxy) radical (TEEPONE) was used successfully for tridimensional EPR and MRI in vivo imaging of mouse head, with a reported half-life of over 80 min. We decided to investigate the stability of tetraethyl-substituted piperidine nitroxides in the presence of hepatic microsomal fractions, since no detailed study of their “metabolic stability” at the molecular level had been reported despite examples of the use of these nitroxides in vivo. In this context, the rapid aerobic transformation of TEEPONE observed in the presence of rat liver microsomal fractions and NADPH was unexpected. Combining EPR, HPLC-HRMS, and DFT studies on a series of piperidine nitroxides — TEEPONE, 4-oxo-2,2,6,6-tetramethyl(piperidin-1-yloxy) (TEMPONE), and 2,2,6,6-tetraethyl-4-hydroxy(piperidin-1-yloxy) (TEEPOL), we propose that the rapid loss in paramagnetic character of TEEPONE is not due to reduction to hydroxylamine but is a consequence of carbon backbone modification initiated by hydrogen radical abstraction in alpha position to the carbonyl by the P450-Fe<sup>(V)</sup>=O species. Besides, hydrogen radical abstraction by P450 on ethyl substituents, leading to dehydrogenation or hydroxylation products, leaves the aminoxyl function intact but could alter the linewidth of the EPR signal and thus interfere with methods relying on measurement of this parameter (EPR oximetry).

**Graphical abstract**

**Keywords:** aminoxyl radical, nitroxyl radical, piperidine nitroxide, TEEPONE, TEEPOL, TEMPONE, spin probe, electron paramagnetic resonance (EPR), electron spin resonance (ESR), microsomes, cytochrome P450

**Abbreviations**

BSA, bovine serum albumin; carbamoyl-PROXYL, 3-carbamoyl-2,2,5,5-tetramethylpyrrolidin-1-yl-oxyl; DFT, Density Functional Theory; DMSO, dimethylsulfoxide; DPI, diphenyliodonium chloride; DTPA, diethylene triamine tetraacetic acid; EPR, electron paramagnetic resonance (equivalent to ESR, electron spin resonance); ESI<sup>+</sup>, electrospray ionization in positive ionization detection mode;  $K_s$ , spectroscopic (apparent) equilibrium dissociation constant; hfc, hyperfine coupling constant; HPLC, high-performance liquid chromatography; HRMS, high-resolution mass spectrometry; MRI, magnetic resonance imaging; P450, cytochrome P450; SOD, superoxide dismutase; TEEPONE, 2,2,6,6-tetraethyl-4-oxo(piperidin-1-yl-oxyl); TEEPOL, 2,2,6,6-tetraethyl-4-hydroxy(piperidin-1-yl-oxyl); TEMPONE, 2,2,6,6-tetramethyl-4-oxo(piperidin-1-yl-oxyl); RLM, rat liver microsomes; RT, retention time.

**Introduction**

Aminoxyl radicals (nitroxides) have a broad range of biological applications [1], from antioxidants [2] and contrast or polarization agents for MRI [3], to spin labels [4] and spin probes of oxygen [5], pH [6], viscosity, or redox status [7,8] in EPR spectroscopy. In many of these applications, the persistence of the radical character of the nitroxide function is essential. The uncommon nitrogen-oxygen 3-electron  $\pi$  bond affords resonance stabilization. Therefore, radical dimerization, reaction with molecular oxygen, or hydrogen atom abstraction are not favored, contributing to stability and longer shelf-life.

The exhaustive substitution by alkyl groups at  $\alpha$ -position to the nitrogen also prevents disproportionation [9]. However, nitroxides can be oxidized to N-oxoammonium cations or reduced to hydroxylamines, both reactions leading to the loss of EPR signal. The formation of N-oxoammonium cation intermediate has been highlighted in the SOD-mimic activity of piperidine and pyrrolidine nitroxides [10], but it is generally accepted that intracellular reduction of nitroxides to hydroxylamines is the primary metabolic pathway limiting applications in biological systems [11].

In-depth studies using various models or integrated systems showed that several mechanisms are involved in the reduction of tetramethyl-substituted nitroxides, depending on the tissue of interest and on the subcellular localization, hence on the lipophilicity and charge of the nitroxide. Cells do not significantly reduce charged compounds that do not permeate cell membranes [12]. Ring type and ring substituents, to a minor extent, influence the reduction rate in the cytosol of hepatocytes and kidney cells with high ascorbate content, piperidine derivatives being reduced faster [12,13]. Thiols are not directly involved in reduction processes but can act as secondary electron donors [14]. Enzyme-mediated reduction appears as preponderant in most cell types, involving either enzymes of the mitochondrial electron transport chain [15–17], NAD(P)H-dependent systems in microsomal fractions [18,19], or soluble enzymes of the hexose phosphate shunt [20].

Considerable research efforts have been taken to improve the resistance of nitroxides against reduction, with variations of ring types (piperidine, pyrrolidine, pyrroline, imidazolidine, and isoindoline), substituents (charged or neutral), and of steric shielding at  $\alpha$ -position to the nitroxide (methyl, cyclohexyl, or ethyl groups) [21–27]. In particular, it has been recently shown that piperidine derivatives with tetraethyl substituents flanking the nitroxide function are reduced by ascorbate at a slower rate than their tetramethyl counterparts [24,26,28]. This property was attributed to steric shielding and a lower reduction potential of the nitroxide, with support of computational studies [29–32]. TEEPONE and TEEPOL (Figure 1) demonstrated high stability in human plasma and in the presence of quiescent and activated human neutrophils [33]. Only slow reduction was also observed in cytosolic extracts of *Xenopus laevis* oocytes and after injection into such oocytes [28]. After intravenous injection, the half-lives measured in the mouse tail reached  $16.4 \pm 1.3$  min and  $20.0 \pm 3.0$  min for TEEPONE and TEEPOL, respectively [31], while tetramethyl counterparts could not be detected. For comparison, the half-life of carbamoyl-PROXYL (3-carbamoyl-2,2,5,5-tetramethylpyrrolidin-1-yl-oxyl) did not exceed  $8.5 \pm 2.7$  min under the same conditions [31]. TEEPONE was thus used for brain EPR and MRI imaging studies (with a reported half-life in the brain over 80 min) [34–36]. Interestingly, in the study by Kinoshita *et al.* [31], the level of signal due to TEEPONE was considerably lower than that of TEEPOL for the same injection dose, both in the mouse tail and in tissue homogenates (including the brain). After reoxidation by ferricyanide addition, the levels of TEEPOL in homogenates (especially in the liver and kidney) were higher than those of tested tetramethyl derivatives. However, levels of TEEPONE remained low under the same conditions whatever the tissue, suggesting that reduction did not contribute significantly to the loss of signal in this case.

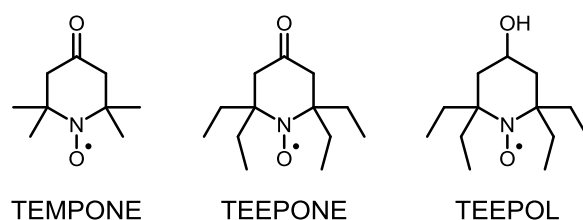


**Figure 1:** Structures of aminoxyl radicals used in this study.

To our knowledge, this peculiar behavior of TEEPONE *in vivo* remains unexplained. Therefore, we decided to further investigate the “metabolic stability” of a series of piperidine nitroxides - TEMPONE, TEEPONE, and TEEPOL (Figure 1), in the presence of microsomal fractions of rat liver under different experimental conditions. These subcellular fractions obtained by homogenization and centrifugation of rat liver are standard tools for *in vitro* metabolic studies. They contain all the membrane-bound enzymes responsible for the metabolism of xenobiotics, such as cytochromes P450 and associated reductases [37], and the use of specific cofactors and inhibitors helps to unravel the enzymatic systems involved in xenobiotic transformation.

## Materials and Methods

### *Reagents*

TEEPONE and TEEPOL were synthesized as orange oils according to previously published protocols with few modifications [26,36]. Purity was assayed by high performance liquid chromatography (HPLC) coupled to high-resolution mass spectrometry (HRMS) and was above 98% (Supplementary figures S1 and S2, and supplementary tables T1 and T2 in Supplementary material). 10-50 mM stock solutions of these nitroxides in DMSO were further diluted in phosphate buffer (The final DMSO concentration in buffer was 0.1% v/v for EPR or 1% v/v for HPLC-HRMS). NADPH, NADH, TEMPONE, diethylene triamine pentaacetic acid (DTPA), and diphenyliodonium chloride (DPI) were purchased from Sigma-Aldrich (St. Quentin Fallavier, France). All other chemicals and solvents were of the highest grade commercially available. Ultrapure water (ELGA, Antony, France, resistivity: 18.2 M $\Omega$ -cm) was used for the preparation of potassium phosphate buffer (0.1 M, pH 7.4) containing 1 mM DTPA, which was used for all experiments unless otherwise stated.

### *Preparation of rat liver microsomes*

The animal study was approved by Paris Descartes University Animal Ethics Committee (CEEA 34), adhering to the French regulations and the European Communities Council Directive on the protection of animals used for scientific purposes. It was authorized by the French Ministry of Higher Education and Research under reference number APAFIS#7494-2016102716338280 v2.

Male Sprague Dawley rats (200–250 g, Charles River, L'Arbresle, France) were provided laboratory chow and water *ad libitum*. After 7 days of adaptation, animals were treated with phenobarbital (20 mg kg<sup>-1</sup>, in corn oil, intraperitoneally for 4 days). Rat liver microsomes (RLM) were prepared by differential centrifugation as previously reported [38]. A single batch of RLM was divided in multiple aliquots and stored at -80 °C until use. Undiluted aliquots were kept on ice during the experiments, used within a couple of hours, and leftovers were discarded to ensure constant enzyme activity throughout the study. Protein concentrations were determined by the Bradford assay with bovine serum albumin (BSA) as a standard [39]. Cytochrome P450 contents were determined by the method of Omura and Sato [40]. The cytochrome c reductase activity was assayed using the protocol of Vermilion and Coon [41] and corresponded to 0.45  $\pm$  0.15  $\mu$ mol cyt c reduced min<sup>-1</sup> mg<sup>-1</sup> protein.

### *Spectral interaction studies*

Absorption difference spectra were recorded at 21°C in a UV-2700 UV-Vis spectrophotometer (Shimadzu, Marne-La-Vallée, France). Small volumes of 10<sup>-4</sup> - 5·10<sup>-1</sup> M stock solutions of nitroxides were added to 1-cm path length sample cuvettes, which contained 150  $\mu$ l of a 2 micromolar P450

microsomal preparation in potassium phosphate buffer (0.1 M, pH 7.4) containing DTPA (1.0 mM). The same amount of buffer was added to the reference cuvette, which contained the same microsomal preparation. The difference spectra were recorded immediately after the addition of nitroxide. Typical type I spectra with peaks at about 390 nm and troughs at about 420 nm were observed. The changes in absorbance were measured as differences in absorbance values at these two wavelengths ( $\Delta A = A_{390} - A_{420}$ ). Apparent dissociation constants ( $K_s$ ) were estimated from plots of the absorbance differences versus concentration by fitting the data to the following equation  $\Delta A = \frac{\Delta A_{max} \times [\text{nitroxide}]}{K_s + [\text{nitroxide}]}$  using KaleidaGraph 4.0 (Synergy Software). (In the case of TEMPONE, absorption of the nitroxide interfered with the measurement above 2 mM. Therefore, only the sample cuvette contained the microsomal preparation, while the reference cuvette was filled with buffer. Then TEMPONE was added to both cuvettes.)

### *EPR spectroscopy*

The samples were prepared by diluting a stock solution of nitroxide and the RLM preparation to the final concentrations of 10-100  $\mu\text{M}$  nitroxide and 1.0  $\mu\text{M}$  P450 in potassium phosphate buffer (0.1 M, pH 7.4) containing DTPA (1.0 mM). When NADPH or NADH were used, their final concentration was 1.0 mM. The samples were prepared by addition of NAD(P)H as last, before mixing and transferring to glass microcapillary pipettes (50  $\mu\text{l}$ , Hirschmann). The capillaries were sealed with CRITOSEAL paste (Leica), placed in a 4-mm quartz tube, and then in the EPR cavity.

EPR measurements were performed using an Elexsys E500 EPR spectrometer (Bruker, Wissembourg, France), operating at X-band (9.8 GHz) and equipped with an SHQ high-sensitivity cavity. Typical settings used were: microwave power, 10 mW; modulation frequency, 100 kHz; modulation amplitude, 0.10 mT for TEMPONE and TEEPONE or 0.15 mT for TEEPOL; receiver gain, 60 dB; time constant, 40.96 ms; conversion time, 41.04 ms; datapoints, 1024; sweep width, 6 mT; sweep time, 42.02 s. EPR spectra were recorded sequentially at 21 °C. Data acquisition and processing were performed using Bruker Xepr software.

### *EPR spectra simulations and extraction of kinetic evolutions*

Computer simulations of EPR spectra were performed using Matlab software (Mathworks) and the dedicated toolbox EasySpin (garlic function) [42]. When indicated kinetic evolutions of mixtures of species were extracted from temporal series of EPR spectra by the pseudo-inverse method described by Lauricella *et al.* [43].

### *HPLC-HRMS study*

Samples (final volume 100  $\mu\text{l}$ ), containing 100  $\mu\text{M}$  nitroxide, RLM diluted to 1.0  $\mu\text{M}$  P450, and 1.0 mM NADPH, were prepared in potassium phosphate buffer (50 mM, pH 7.4). Each sample was incubated for the indicated period of time (0-60 min) at 21 °C, before acetonitrile (50  $\mu\text{l}$ ) was added to stop the reaction. The precipitate was separated by centrifugation (20 min at 13000 rpm on microcentrifuge miniSpin, Eppendorf) before HPLC-HRMS analysis. Control samples were prepared, without NADPH or nitroxide, respectively.

HPLC-HRMS analyses were performed on a Thermo Exactive Orbitrap spectrometer (Thermo Scientific, Les Ulis, France) coupled to a Nexera X2 HPLC (Shimadzu, Marne-La-Vallée, France) system using a Cluzeau Satisfaction RP 18-AB column (150x2.0 mm, 3  $\mu\text{m}$ , C.I.L. Cluzeau, Sainte-Foy-La-Grande, France), and a gradient of A+B starting at 10% B for 2 min then increasing linearly to 20% B in 4 min, then to 50% B in 2 min, then to 100% B in 2 min for 7.9 min, then back to 10% B at 18 min, and

equilibration at 10% B for 7 min (A = mQ water plus 0.1% HCOOH, and B = CH<sub>3</sub>CN/H<sub>2</sub>O/HCOOH (949:50:1) at 200  $\mu$ L/min). Mass spectra were obtained by electrospray ionization in positive ionization detection mode (ESI<sup>+</sup>) under the following conditions: sheath gas 15, auxiliary gas 5, capillary temperature 275°C, capillary voltage 42.5 V, tube lens 60 V, skimmer 16 V; and mass range 150–520, and HCD (higher-energy collisional dissociation) and CID (collision induced dissociation) disabled, resolution 10000.

The mass spectra of pure TEEPONE (Supplementary Figure S1 and Table T1) and TEEPOL (Supplementary Figure S2 and Table T2) show a similar ionization pattern with three ions of comparable intensity at  $m/z = M, M+1,$  and  $M+2$ , typical of electrospray ionization of nitroxides and positive detection mode [44].

### *Computational details*

All theoretical calculations were based on the Density Functional Theory (DFT) and were performed with the ORCA program package [45]. Full geometry optimizations as well as electronic structure calculations were undertaken for all systems using the hybrid functional B3LYP [46,47] in combination with the TZV/P [48] basis set for all atoms, and by taking advantage of the resolution of the identity (RI) approximation in the Split-RI-J variant [49] with the appropriate Coulomb fitting sets [50]. Increased integration grids (Grid4 and GridX4 in ORCA convention) and tight SCF convergence criteria were used in the calculations. To ensure that the resulting structures converged to a local minimum on the potential energy surface, numerical frequency calculations were performed and resulted in only positive normal vibrations. Solvent effects were accounted for according to the experimental conditions. For that purpose, we used water as a solvent ( $\epsilon = 80$ ) within the framework of the conductor like screening (COSMO) dielectric continuum approach [51]. The bond dissociation energies (BDE) were computed from the gas-phase optimized structures as a sum of electronic energy, solvation and thermal corrections to the free energy. EPR parameters were obtained from additional single-point calculations using the EPR-II basis set [52] and the hybrid functional B3LYP. Preliminary calculations showing a net underestimation of the magnitude of the nitrogen hyperfine coupling constant (hfc), we conducted a calibration study using TEEPONE as a reference compound. We constructed and optimized new model systems by including from one to five water molecules in the surrounding of TEEPONE. We then evaluated the influence of explicit solvent molecules on the prediction of such EPR parameters as it was suggested that the nitrogen hfc is influenced not only by the polarity of the solvent, but also by the formation of solute-solvent hydrogen bonds (data shown in Supplementary Figure S4 and Table T3) [53]. Our results indicated that the model system together with four water molecules is converged and gives the best correlation between experiment and theory. Molecular orbitals were generated using the *orca\_plot* utility program and optimized structures were both visualized with the Chemcraft program.

## **Results and discussion**

### *EPR study of piperidine nitroxides in incubations with RLM*

Figure 2 summarizes the EPR observations obtained upon aerobic incubations of 10  $\mu$ M nitroxide with RLM (0.57 mg ml<sup>-1</sup> protein, 1  $\mu$ M P450) in the presence of NADPH in potassium phosphate buffer (0.1 M, pH 7.4, containing 1 mM DTPA) at 21°C.

In the case of TEMPONE, only a slow decrease in intensity without change in the shape of the spectrum was observed ( $\approx 0.5 \text{ nmol min}^{-1} \text{ mg}^{-1} \text{ protein}$ ) (Figure 2A). This decay was RLM- and NADPH-dependent, and was enhanced by prior saturation of the microsomal preparation with carbon monoxide (CO), a ligand of P450-Fe(II) (results not shown). These results point out to reduction of the nitroxide function by reductases present in RLM and not to P450 activity, which is in agreement with previous studies with tetramethyl-substituted piperidine nitroxides [19,54].

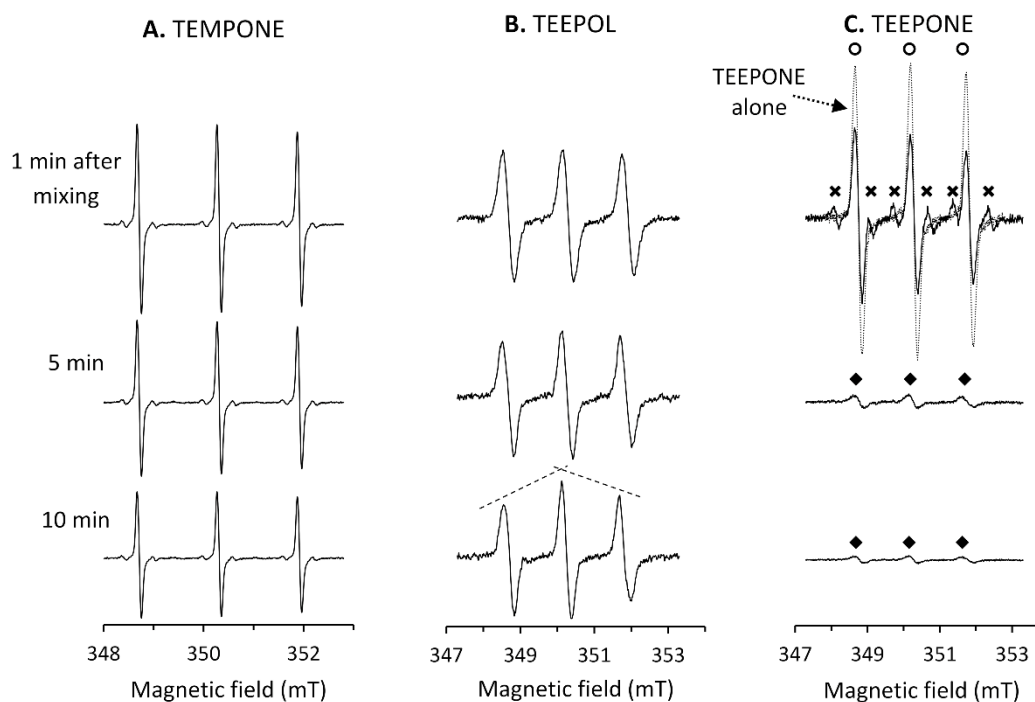


**Figure 2:** EPR study of aerobic incubations of nitroxides ( $10 \mu\text{M}$ ) with RLM ( $0.57 \text{ mg ml}^{-1} \text{ protein}$ ,  $1.0 \mu\text{M}$  P450) and NADPH ( $1 \text{ mM}$ ) at  $21 \text{ }^\circ\text{C}$  at different incubation times. The samples were prepared in potassium phosphate buffer ( $100 \text{ mM}$ ,  $\text{pH } 7.4$ , containing  $1 \text{ mM}$  DTPA) by addition of NADPH stock as last. **A.** Case of TEMPONE; **B.** Case of TEEPOL; **C.** Case of TEEPONE (The spectrum of TEEPONE alone was overlaid with the spectrum obtained right after mixing to highlight the fast initial changes in the signal. At least three species can be observed during the reaction: TEEPONE (open circles), a 6-line intermediate (crosses), and a 3-line species (closed diamonds). Experimental details and EPR settings are described in the experimental section.

In the case of TEEPOL, a slow distortion of the EPR spectrum was observed, with a characteristic “roof effect” (Figure 2B). This could be explained by overlapping of the EPR spectrum of one (or several) different nitroxide product(s) with a slightly smaller nitrogen coupling constant with that of the starting nitroxide. The middle lines of all nitroxides being almost in the same position and the low- and high-field lines having slightly different positions, low- and high-field lines would appear broadened. A similar effect was reported in a study where TEMPONE was transformed to TEMPOL in isolated perfused rat liver [55]. The change in the observed  $g$ -value ( $0.0027$  units during the course of the experiment) comforts our hypothesis of a combination of nitroxides with overlapping signals. Despite this extensive evolution, the new nitroxide species demonstrated a good stability and the EPR signal with the typical “roof effect” was visible over several hours of incubation. Precise evolution kinetics could not be extracted due to heavy overlapping and incomplete transformation. The overall intensity of the EPR spectrum decreased very slowly with time, which suggests that reduction of the nitroxide group to hydroxylamine is not a major pathway to interpret the results. Instead, a modification of other parts in TEEPOL structure is expected.



The case of TEEPONE was even more puzzling. No reaction was observed when either microsomes or NADPH was omitted. But, right after preparation of an aerobic mixture of the nitroxide with both RLM and NADPH, a rapid decay of TEEPONE (identified with open circles in Figure 2C) was observed with appearance of an overlapping transient six-line radical species (crosses in Figure 2C) where the single electron coupled with both one nitrogen and one hydrogen atom. Four minutes after sample preparation, the starting nitroxide TEEPONE was almost completely exhausted unveiling the weak signal of a new nitroxide species (closed diamonds in Figure 2C) with a slightly smaller nitrogen coupling constant and larger linewidth. This new three-line nitroxide was not a subject of rapid metabolism, its signal decaying slowly. The spectral properties and kinetic evolution of the different species were extracted from the temporal series of EPR spectra using EasySpin and the pseudo-inverse method [43] and are presented in Table 1 and Figure 3, respectively (see also Supplementary Figure S3 for simulations of EPR spectra).

**Table 1:** Spectral characteristics of the different species observed in the aerobic reaction of TEEPONE with RLM and NADPH, as identified in Figure 2C. The hyperfine coupling constants ( $A_N$ ,  $A_H$ ) and linewidth parameter ( $\Delta B$ ) were extracted by simulation with EasySpin [42]. Calculated spectra are presented in Supplementary Figure S3.

	<b>TEEPONE</b> <b>(o)</b>	<b>6-line intermediate</b> <b>(x)</b>	<b>3-line species</b> <b>(◆)</b>
<b><math>A_N</math> (mT)/(MHz)</b>	1.54/43.2	1.67/46.8	1.50/42.0
<b><math>A_H</math> (mT)/(MHz)</b>	-	0.95/26.6	-
<b><math>\Delta B</math> (mT)</b>	0.20	0.16	0.36

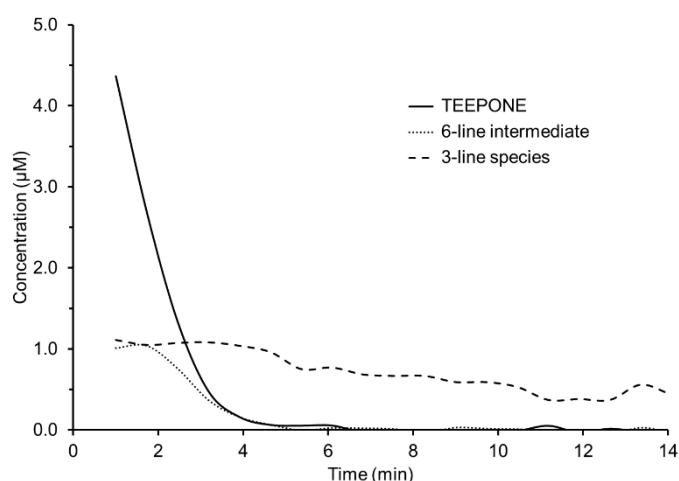


**Figure 3:** Kinetic evolutions of the different species observed in Figure 2C (extracted from the temporal series of EPR spectra by the pseudo inverse method [43]).

To unravel the underlying mechanism of transformation of TEEPONE, we performed supplementary experiments with different cofactors and inhibitors, which are presented in Table 2.

**Table 2:** Initial rates of decrease of TEEPONE and formation of the 6-line intermediate in incubations with RLM in the presence of various cofactors and inhibitors. The samples were prepared in potassium phosphate buffer (100 mM, pH 7.4, containing 1 mM DTPA) by addition of NAD(P)H stock as last. The incubations were performed at 21 °C.

Experimental conditions	Initial rate of decrease of TEEPONE (nmol min <sup>-1</sup> mg <sup>-1</sup> prot)	Initial rate of decrease of TEEPONE (nmol min <sup>-1</sup> nmol <sup>-1</sup> P450)	Formation of the 6-line intermediate
TEEPONE (100 μM) + RLM (1 μM P450) + NADPH (1 mM)	7.7 ± 0.2 (n = 2)	4.4 ± 0.2 (n = 2)	+
- NADPH	0.0	0.0	-
+ CO*	1.7	1.0	-
+ DPI (100 μM) <sup>#</sup>	3.0	1.7	+
- NADPH + NADH (1 mM)	0.9	0.5	+
+ NADH (1 mM)	10.1	5.8	+

\* RLM were treated with gaseous CO prior to addition of the nitroxide.

<sup>#</sup> RLM were briefly mixed with a fresh solution of DPI prior to addition of the nitroxide.

When TEEPONE was incubated with RLM supplemented with NADPH, it decayed very fast with an initial rate of 7.7 ± 0.2 nmol min<sup>-1</sup> mg<sup>-1</sup> protein. The reaction was RLM- and NADPH-dependent. Pretreatment of RLM with CO reduced the initial decay rate and prevented the formation of the six-line intermediate. Moreover, potassium ferricyanide addition did not regenerate TEEPONE signal. This indicates that the formation of the six-line intermediate depends on P450 heme center and that direct reduction to hydroxylamine by the reductase is a minor pathway in this case, in opposition to tetramethyl piperidine nitroxides. The reductase inhibitor DPI slowed down the evolution of all species proving the involvement of the whole P450 catalytic cycle. When NADPH was replaced by NADH, a cofactor of cytochrome b<sub>5</sub> reductase, the whole cycle was still functional but the reactions were very slow. It cannot be concluded if cytochrome b<sub>5</sub> catalyzes the same transformation or if the reductase merely transfers electrons to P450 [56]. Expectedly, when both NADPH and NADH were added, the reactions were faster than with any cofactor alone, consistent with a larger inflow of electrons.

#### *HPLC-HRMS study of tetraethyl piperidine nitroxides in incubations with RLM*

To get more insight into these transformations, incubations of TEEPONE and TEEPOL with RLM were studied by HPLC-HRMS.

When TEEPONE was incubated for increasing periods of time with NADPH-supplemented RLM, the corresponding peak eluted at 16.4 min gradually disappeared with concomitant build-up of several other peaks at lower retention time (Figure 4A). The corresponding mass spectra are shown in Figure

5E, as well as the reconstructed chromatograms of the principal ions (Figure 5A-5D). The major identified products correspond to the addition of an oxygen atom, dehydrogenation, isomerization of the starting material, and the loss of an ethyl group (Table 3). Without NADPH, no such transformation occurred, confirming EPR observations.

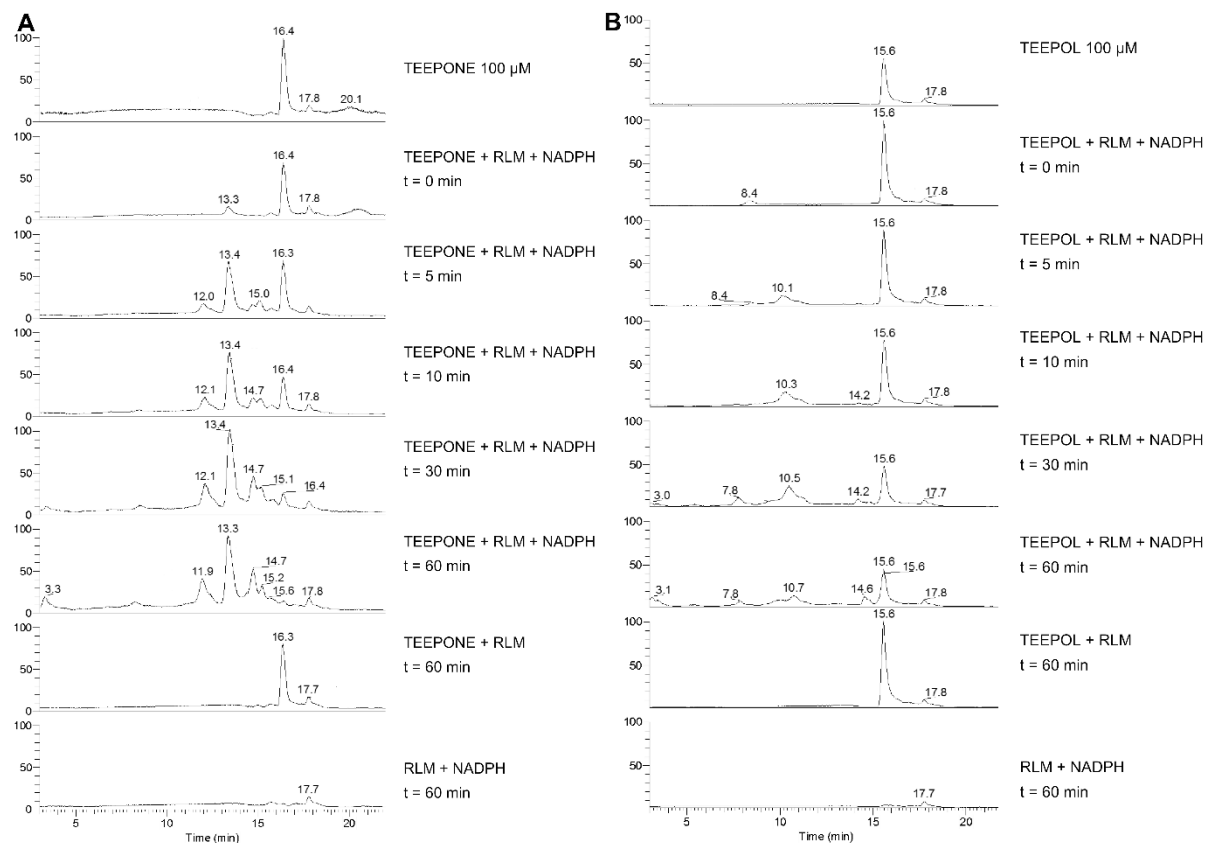


**Figure 4:** HPLC-HRMS study of the incubations of **(A)** TEEPONE and **(B)** TEEPOL (100  $\mu$ M) with or without RLM (1  $\mu$ M P450) and NADPH (1 mM). The samples were prepared as described in the experimental section. The reconstructed chromatograms at  $m/z = 195$ -250 Da are shown for the conditions and indicated time reported on the left. The peak at 17.7-17.8 min can be ignored as it was identified in the blank (RLM + NADPH).

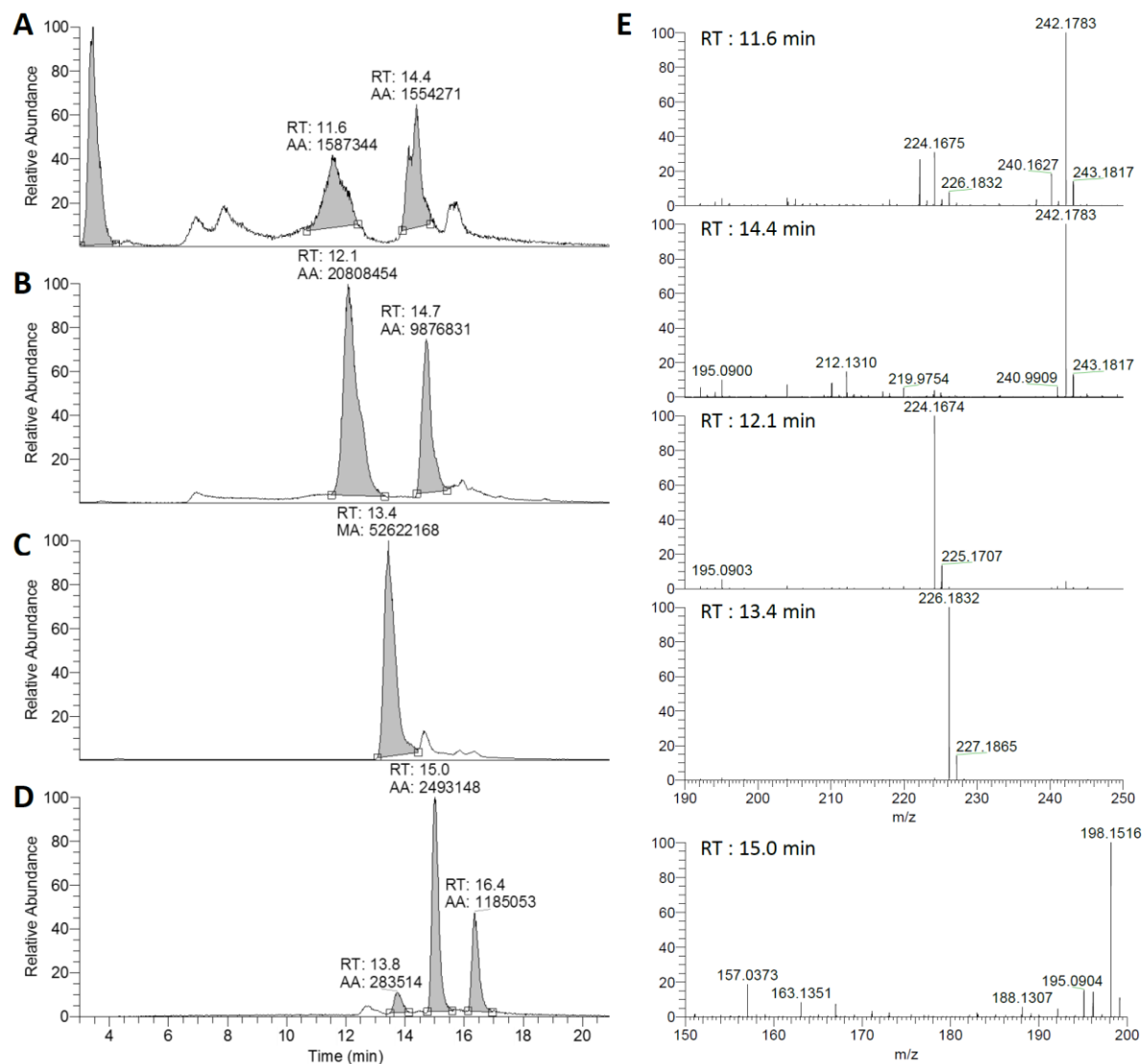


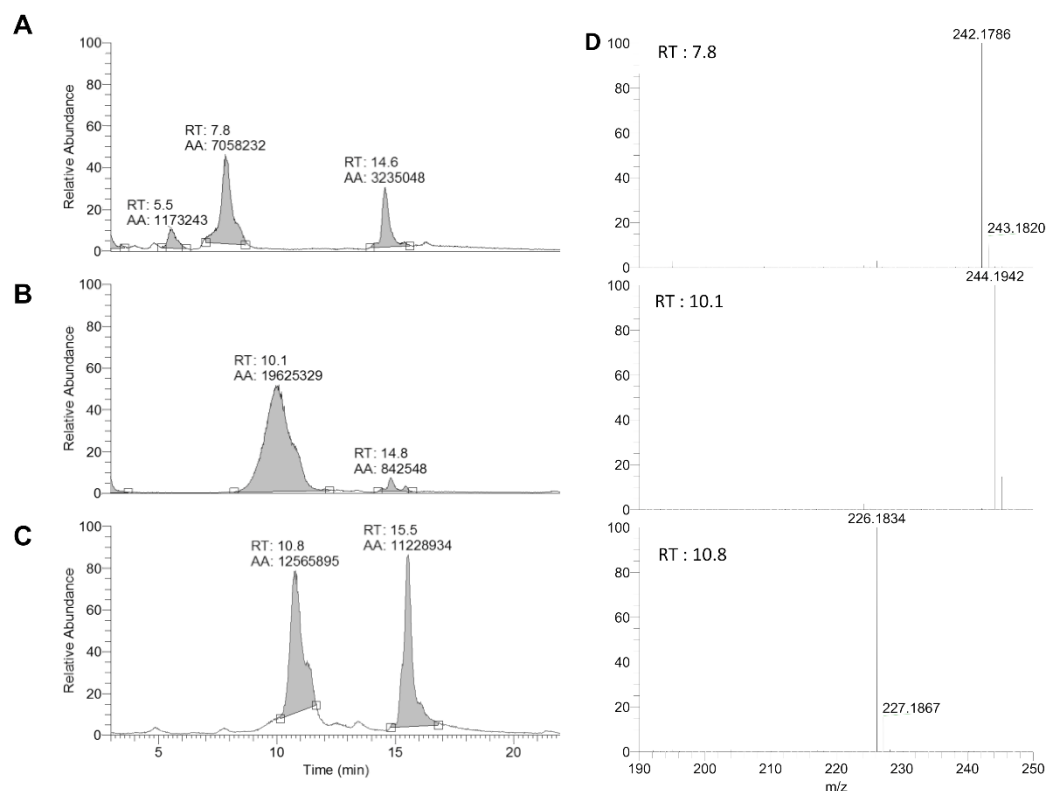
**Figure 5:** HPLC-HRMS study of the incubation of TEEPONE (100  $\mu$ M) with RLM (1  $\mu$ M P450) and NADPH (1 mM) after 30 min. **Panels A-D** show the reconstructed chromatograms at  $m/z = 242.1751$ , 224.1645, 226.1802, and 198.1489, respectively. (MA or AA: peak area). **Panel E** represents the HRMS spectra obtained for the peaks at retention times (RT) 11.6, 14.4, 12.1, 13.4, and 15.0 min, respectively, in panels A-D. The corresponding observed and calculated  $m/z$  values for the indicated elemental composition are reported in Table 3.

**Table 3:** HRMS characteristics of the main products formed upon aerobic incubations of TEEPONE with RLM in the presence of NADPH<sup>a</sup>. (See Figure 8 for proposed formation mechanism.)

RT (min)	m/z (Da)		Chemical formula	Putative structures
	observed	calculated		
11.6 14.4	242.1782	242.1751	C <sub>13</sub> H <sub>24</sub> NO <sub>3</sub> <sup>+</sup> [M <sup>+</sup> ]	<p>Chemical structures 8 and 8' are shown. Structure 8 is a 6-membered ring with a carbonyl group at the top, a nitrogen atom at the bottom with a lone pair and a negative charge, and a hydroxyl group on the right side. Structure 8' is similar but has a hydroxyl group on the left side.</p>
12.1 14.7	224.1674	224.1645	C <sub>13</sub> H <sub>22</sub> NO <sub>2</sub> <sup>+</sup> [M <sup>+</sup> ]	<p>Chemical structure 7 is a 6-membered ring with a carbonyl group at the top, a nitrogen atom at the bottom with a lone pair and a negative charge, and a vinyl group on the right side.</p>
13.4	226.1832	226.1802	C <sub>13</sub> H <sub>24</sub> NO <sub>2</sub> <sup>+</sup> [MH <sup>+</sup> ] <sup>b</sup>	<p>Chemical structures 5 and 3''' are shown. Structure 5 is a 6-membered ring with a carbonyl group at the top, a nitrogen atom at the bottom with a lone pair and a negative charge, and a hydroxyl group on the left side. Structure 3''' is a 6-membered ring with a carbonyl group at the top, a nitrogen atom at the bottom with a lone pair and a negative charge, and a hydroxyl group on the right side.</p>
15.0	198.1516	198.1489	C <sub>11</sub> H <sub>20</sub> NO <sub>2</sub> <sup>+</sup> [MH <sup>+</sup> ]	<p>Chemical structure 4' is a 6-membered ring with a carbonyl group at the top, a nitrogen atom at the bottom with a lone pair and a negative charge, and a hydroxyl group on the right side.</p>

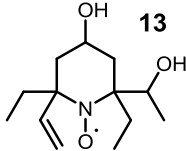
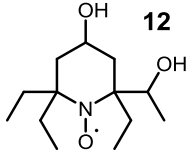
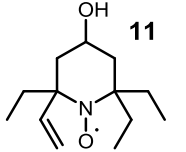
<sup>a</sup> Conditions are described in the experimental section. Mass (in Da) observed or calculated according to the indicated formula for the molecular ion. <sup>b</sup> Note that though the chemical formula is identical to that of the starting material TEEPONE, the product eluted at 13.4 min is easier to ionize and the HRMS spectra in Supplementary Figure S1 and figure 5E (fourth spectrum from top) are different.

The same set of experiments was run with TEEPOL (RT = 15.6 min), which showed slower decay rate over 60 min incubation than TEEPONE (Figure 4B), confirming the results previously obtained by EPR. Three major products of TEEPOL transformation were identified (Figure 6 and Table 4), corresponding to the addition of an oxygen atom (RT = 10.1 min), dehydrogenation (RT = 10.8, 15.5 min), and combination of these reactions (RT = 7.8, 14.6 min), but some appeared in more than one peak, suggesting production of isomers.



**Figure 6:** HPLC-HRMS study of the incubation of TEEPOL (100  $\mu$ M) with RLM (1  $\mu$ M P450) and NADPH (1 mM) after 60 min. **Panels A-C** show the reconstructed chromatograms at  $m/z = 242.1756$ ; 244.1907; and 226.1807, respectively. (AA: peak area). **Panel D** represents the HRMS spectra obtained for the peaks at RT 7.8; 10.1; and 10.8 min, respectively, in panels A-C. The corresponding observed and calculated  $m/z$  values for the indicated elemental composition are reported in Table 4.

**Table 4:** HRMS characteristics of the main products formed upon incubations of TEEPOL by RLM in the presence of NADPH.<sup>a</sup>

RT (min)	m/z (Da)		Chemical formula	Putative structure
	observed	calculated		
7.8 14.6	242.1786	242.1751	C <sub>13</sub> H <sub>24</sub> NO <sub>3</sub> <sup>+</sup> [M <sup>+</sup> ]	
10.1	244.1942	244.1907	C <sub>13</sub> H <sub>26</sub> NO <sub>3</sub> <sup>+</sup> [M <sup>+</sup> ]	
10.8 15.5	226.1834 227.1867	226.1802 227.1880	C <sub>13</sub> H <sub>24</sub> NO <sub>2</sub> <sup>+</sup> [M <sup>+</sup> ] C <sub>13</sub> H <sub>25</sub> NO <sub>2</sub> <sup>+</sup> [MH <sup>+</sup> ]	

<sup>a</sup> Conditions are described in the experimental section. Mass (in Da) observed or calculated according to the indicated formula for the molecular ion.

#### Interpretation and proposed pathways for product formation

In previous studies of nitroxide metabolism by RLM, the P450-catalyzed conversion of tetramethyl piperidine-derived nitroxides to a 2,2-dimethylpyrrolidine moiety has been described (Figure 7) [57]. This reaction was faster with RLM in the absence of NADPH and was also catalyzed by hemin alone.

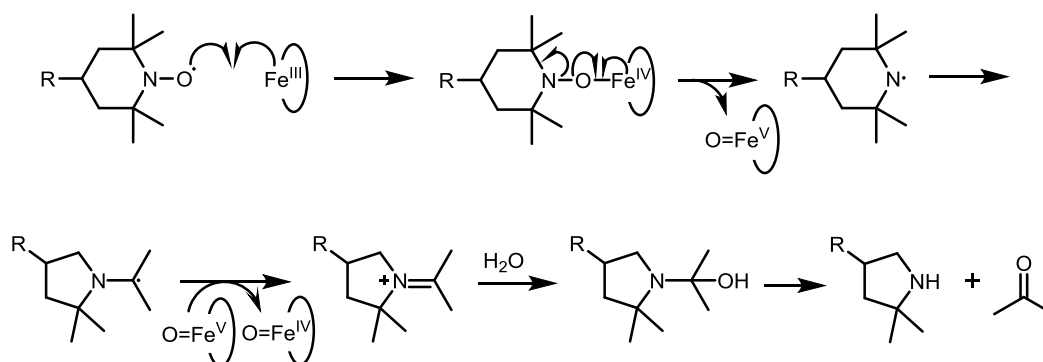


**Figure 7:** Mechanism of the transformation of piperidine-based tetramethyl-substituted nitroxides by ferric heme proposed in reference [57].

The proposed mechanism for this transformation starts with homolytic cleavage of the N-O bond induced by interaction of the nitroxide with ferric heme iron. A nitrogen-centered radical is formed along with a  $\text{Fe}^{\text{V}}=\text{O}$  species. After rearrangement of the nitrogen-centered radical by  $\beta$ -scission, the  $\text{Fe}^{\text{V}}=\text{O}$  species abstracts an electron and forms an iminium cation derivative. Following hydration, this intermediate undergoes N-dealkylation to give 2,2-dimethylpyrrolidine derivative and acetone, which was detected by mass spectrometry.

By contrast, the present transformation of tetraethyl piperidine nitroxides does not involve P450-Fe(III) and is clearly NADPH-dependent. We suspect that the coordination of the  $\text{N-O}^{\bullet}$  moiety to the iron is prevented by increased steric hindrance and the pathway leading to 2,2-dimethylpyrrolidine is not active.

Based on EPR and HPLC-HRMS results and knowledge of P450 activity [58], we propose two different routes for the P450-catalyzed transformation of TEEPONE depending on the site of initial activation. The reduction to hydroxylamine **1** being excluded, the first pathway (A) is fast and produces the transient six-line nitroxide intermediate; the second (B) gives stable nitroxides with different spectral properties (Figure 8). Most of the initial nitroxide is likely metabolized through the fast route (A). In this first route, the molecule is activated by abstraction of an  $\alpha$ -hydrogen to the carbonyl group by  $\text{Fe}^{\text{V}}=\text{O}$ . This position in carbonyl compounds is susceptible to attack by P450. The resulting carbon-centered radical **2** is likely to undergo  $\beta$ -scission and, depending on the bond that breaks, products of ring contraction **3**, dealkylation **4**, or ring opening **5** are expected. Compound **3** would then evolve to **3'** through the "oxygen rebound" mechanism [58]. Nitroxides **3'** and **4** are possible candidates for the six-line intermediate identified by EPR. They are less sterically protected than TEEPONE, which is in favor of a fast reduction to **3''** and **4'**. However, no EPR signal could be recovered by ferricyanide and further decomposition is assumed. Metabolite **5** is EPR silent and can only be detected by mass spectrometry. It cannot be concluded whether the species eluted at 13.4 min corresponds to compound **5** or to **3'''**, a product of intramolecular dehydration of compound **3''**.



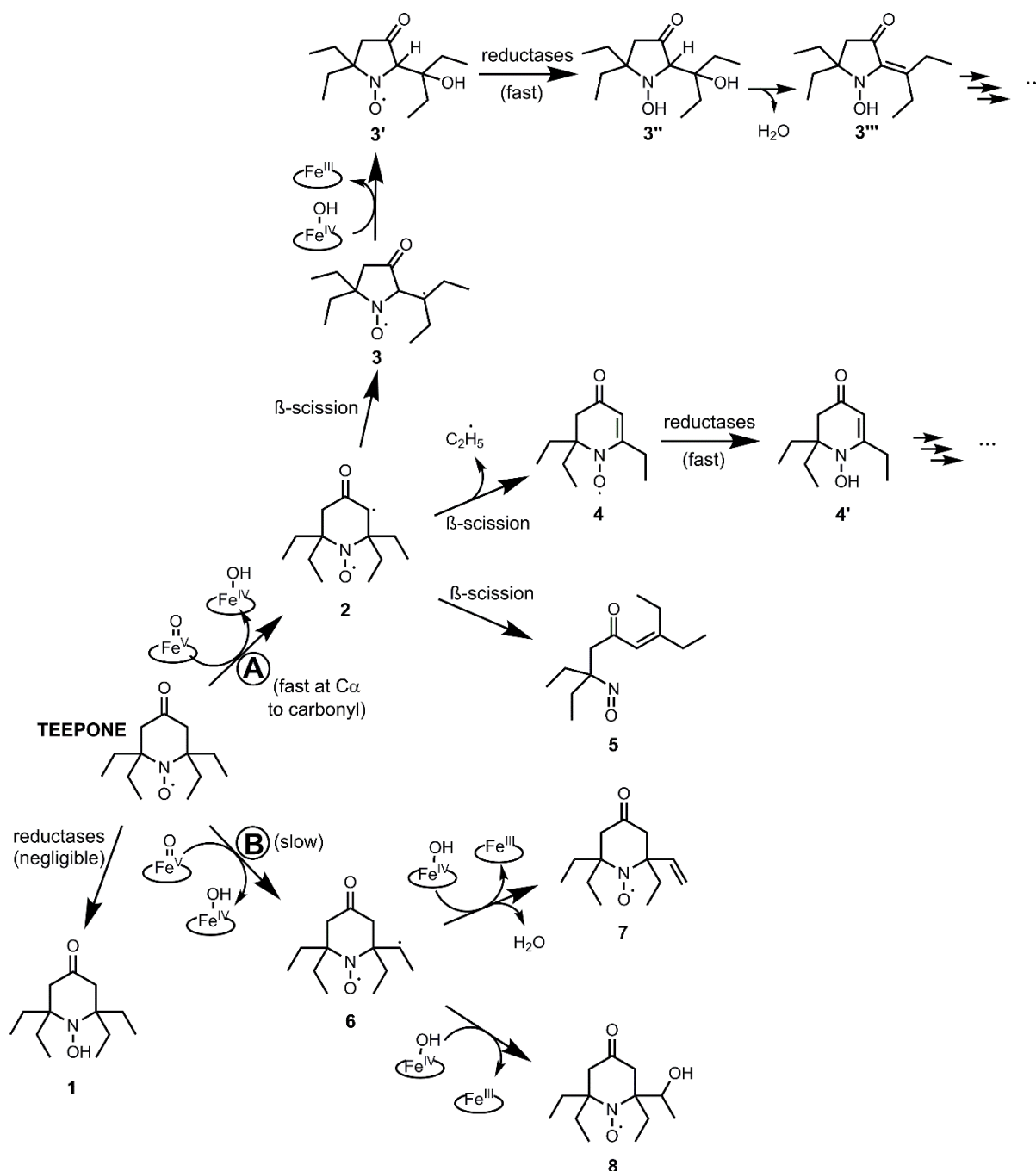


**Figure 8:** Proposed products and corresponding formation pathways A and B in aerobic transformations of TEEPONE by RLM and NADPH.

DFT calculations were conducted on putative structures **3'** and **4** including explicit solvent molecules to determine whether their EPR properties were in agreement with those of the observed six-line species. The DFT-optimized geometry and the singly occupied molecular orbital of **3'** and **4** with four water molecules in their surrounding are presented in Figure 9. Electronic structure calculations show that the unpaired electron is mainly delocalized over the NO moiety and occupies an antibonding  $\pi$ -orbital in both cases.

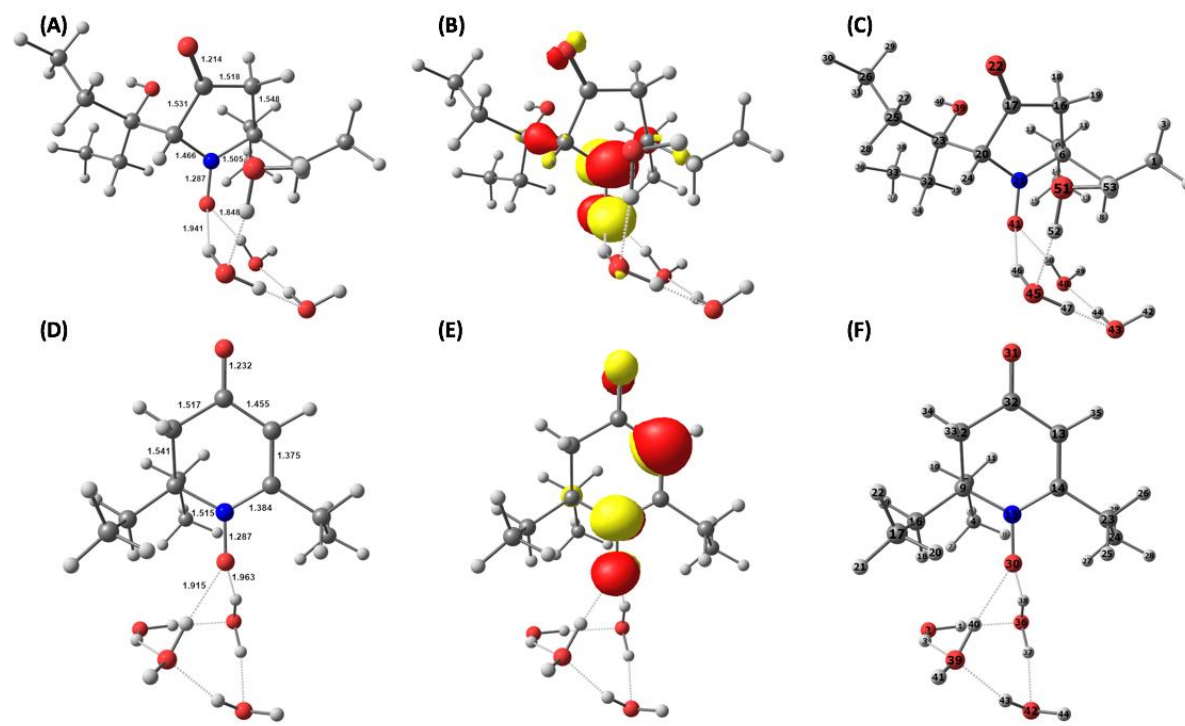


**Figure 9:** DFT-calculated structures for  $3' + 4 \text{H}_2\text{O}$  and  $4 + 4 \text{H}_2\text{O}$ : optimized geometries with selected metrical parameters (Å, **A** and **D**), Singly Occupied Molecular Orbitals (**B** and **E**), and atom numberings (**C** and **F**), respectively.

The computed hyperfine coupling constants for the selected nitrogen and hydrogen centers are reported in Table 5 (See Supplementary Tables T4 and T5 for more details). Our computational results show a pretty fair agreement between theory and experiment for the case of  $3'$  suggesting that this structure is compatible with the one observed by continuous wave EPR spectroscopy (Table 1).

**Table 5:** DFT-calculated hyperfine coupling constants\* (hfcs, MHz) for the geometry-optimized structures  $3' + 4 \text{H}_2\text{O}$  and  $4 + 4 \text{H}_2\text{O}$ .

Structure	$^{14}\text{N}A_{\text{iso}}$	$^1\text{H}A_{\text{iso}}$ [atom number]
$3' + 4 \text{H}_2\text{O}$	44.2	41.0 [24]
$4 + 4 \text{H}_2\text{O}$	26.5	25.9 [35]

\* While hfcs can be in principle either positive or negative, continuous wave EPR will only give access to absolute values. Comparison between experiment and theory thus requires presenting and discussing absolute hfcs.

The second, slower metabolic route (B) (Figure 8) occurs when the molecule is activated by abstraction of a hydrogen atom from one of the ethyl groups to give intermediate **6**. According to calculations of bond dissociation energy for H-atom abstraction, the  $\alpha$ -position to the carbonyl group is more favorable for this reaction than the methylene carbon of the ethyl group (by 8.7 kcal.mol<sup>-1</sup>) or the

terminal carbon ( $12.1 \text{ kcal.mol}^{-1}$ , data shown in Supplementary Figure S6 and Table T6). A similar thermodynamics-driven order of reactivity is usually observed in P450 reactions. The reaction can further proceed either to hydroxylation through the “oxygen rebound” mechanism [58] or through dehydrogenation. Desaturation, or dehydrogenation, is a less common reaction catalyzed by P450 [58]. In all cases of dehydrogenation by P450, hydroxylation of the same position is also present and is usually the major course of the reaction. Both reactions start with hydrogen abstraction by  $\text{Fe}^{\text{V}}=\text{O}$ , then there is a competition between “oxygen rebound” and abstraction of what is formally a second hydrogen (or an electron plus a proton). This mechanism is supported by similar results found in metabolic studies of valproic acid [59] and capsaicin [60]. The resulting nitroxides **7** and/or **8** are more stable than starting compound TEEPONE and could correspond to the 3-line species observed at the end of the reaction. We assume they are no longer substrates for the fast metabolism (route A), due to a modified affinity to P450 compared to TEEPONE.

Despite the presence of a carbonyl function in TEMPONE, this nitroxide is solely reduced by reductases at a slow rate and is not transformed by P450 following pathway A. A possible explanation is the large difference in lipophilicity of the nitroxides, a parameter that greatly influences the affinity of drugs for P450 active site [61]. Kinoshita et al. [31] reported the octanol/water partition coefficients ( $P_{o/w}$ ) of TEMPONE and TEEPONE as  $1.90 \pm 0.17$  and  $139.17 \pm 3.77$ , respectively. We confirmed this hypothesis by testing the spectral interactions of both nitroxides with P450 [62,63]. Typical type I difference spectra with maximum at about 390 nm and minimum at about 424 nm (i.e., blue shifts of the Soret band of the heme cofactor) were observed in both cases (Figure 10). This is the sign of an increased high spin character of the P450- $\text{Fe}^{\text{III}}$  resting state upon ligand binding (typically observed when the coordinated water ligand is removed from the active site). The spectroscopic equilibrium dissociation constant was dramatically higher for TEMPONE ( $K_s \approx 0.8 \pm 0.3 \text{ mM}$ ), than for TEEPONE ( $K_s \approx 9.3 \pm 1.9 \text{ }\mu\text{M}$ , Figure 10), consistent with a smaller binding affinity.

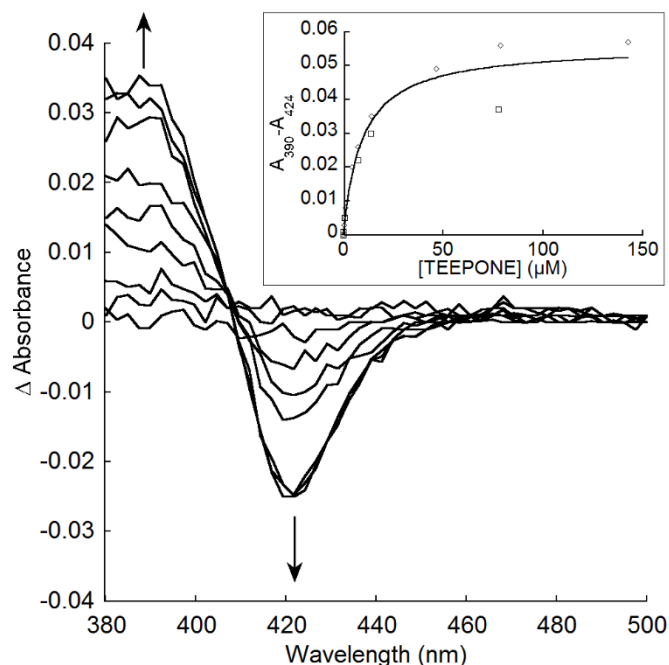


**Figure 10:** Type I spectral changes with TEEPONE. **Main.** Difference spectra caused by addition of TEEPONE to RLM. Additions of TEEPONE to the sample cuvette were 0.40, 0.96, 4.25, 10.9, 17.3, 49.7, 82.0, 145.9  $\mu\text{M}$ . **Inset.** TEEPONE dependence of Type I spectral changes ( $n=2$ ). The experimental data

were fitted to  $\Delta A = \frac{\Delta A_{max} \times [\text{nitroxide}]}{K_s + [\text{nitroxide}]}$  with  $\Delta A_{max} = 0.056 \pm 0.003$  and  $K_s = 9.3 \pm 1.9 \mu\text{M}$ . See experimental section for details.

Pathway A is excluded in the case of TEEPOL because of the lack of carbonyl group, while reduction to hydroxylamine **9** is unlikely (Figure 11). Therefore, only products of dehydrogenation and hydroxylation on ethyl groups **11** and **12**, and combination of both **13** were detected by HPLC-HRMS as several peaks suggesting formation of isomers (Figures 4B and 6 and Table 4) and resulting from transformation route B (Figure 11). The binding affinity of TEEPOL to the P450 active site (Type I,  $K_s \approx 53 \pm 37 \mu\text{M}$ ) was slightly smaller than that of TEEPONE, their lipophilicity being close ( $P_{o/w} = 214.22 \pm 7.83$  for TEEPOL [31]). Oxidation of the alcohol function in TEEPOL cannot be considered as a significant pathway, because we would have expected the TEEPONE product to be rapidly transformed by P450, which would have led to a rapid extinction of EPR signal in contradiction with the present observations.

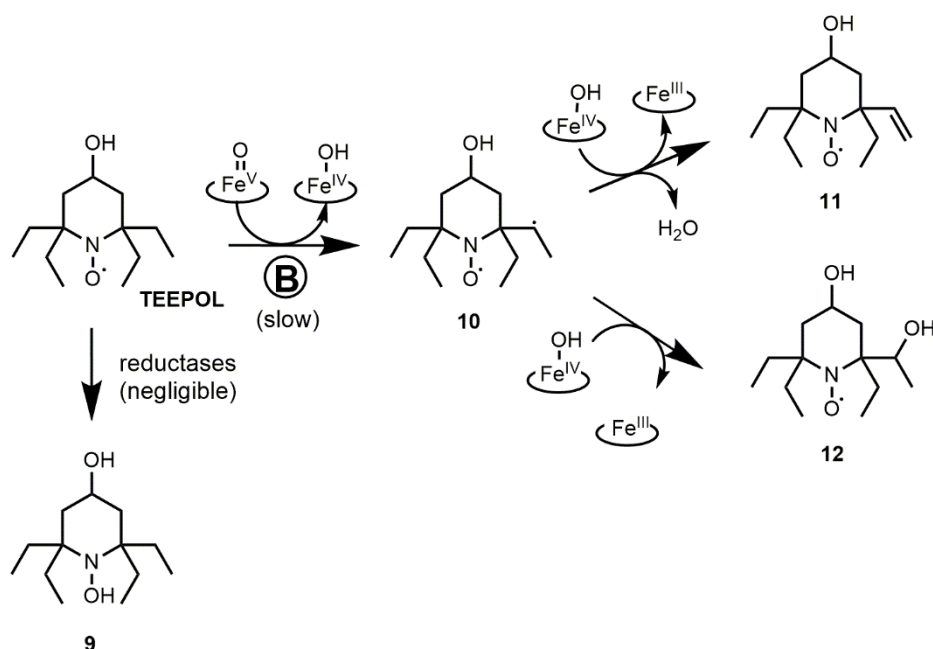


**Figure 11:** Proposed products and corresponding formation pathways in aerobic transformations of TEEPOL by RLM and NADPH.

## Conclusions

The metabolism of tetramethyl-substituted cyclic nitroxides was extensively studied in the 1980s-90s and reduction processes, mediated by enzymes of the mitochondrial electron transport chain or by small molecules such as ascorbate, were identified as major pathways of transformation of these structures both in cells and in vivo [12,13,15–17]. It has been generally assumed that the same principles would apply to newly developed tetraethyl-substituted analogs and that protection of the structures against reduction would afford metabolic stability of the nitroxides. In contradiction with this common belief, the present work sheds light on a new, rapid, and specific transformation of TEEPONE catalyzed by P450 and most likely initiated by hydrogen atom abstraction by  $\text{P450-Fe}^{\text{V}}=\text{O}$  species in  $\alpha$ -position to the carbonyl, with irreversible destruction of the probe. This process could not

be identified in the previous study by Jagtap *et al.* using *Xenopus laevis* oocytes [28], because frog embryos have limited xenobiotic metabolism through early stages of development [64]. Our results suggest that TEEPONE will be rapidly processed in organs with high P450 content, such as the liver and kidney [65]. In the study by Kinoshita *et al.* [31], levels of TEEPONE in these organs were indeed dramatically lower than that of TEEPOL injected at the same dose in mice, especially after reoxidation by ferricyanide. The percentage doses of TEEPONE and TEEPOL after reoxidation by ferricyanide in the brain were much more similar [31]. Moreover, TEEPONE was successfully used for *in vivo* MRI and EPR imaging in the mouse brain, with an apparent half-life over 80 min [34–36]. P450 enzymes display different tissue distributions and certain substrate selectivity, although a substrate may be metabolized by more than one enzyme. We did not study the P450 isoform-dependence, but those present in the brain might be less efficient at processing TEEPONE. This interpretation should, however, be treated with caution because the nitroxide was formulated in a lipid emulsion for intravenous injection in the imaging studies [34–36] without evaluation of the dynamics of probe release from the emulsion, which means that the measured half-life may not be a true reporter of the metabolic stability of TEEPONE in the mouse brain.

Nitroxides with narrow EPR lines are essential for low-frequency EPR spectroscopy and *in vivo* EPR imaging. From this point of view, TEEPONE can be considered a better probe than TEEPOL, its EPR linewidth being smaller (0.2 vs 0.3 mT) [26]. The effect of structure on EPR linewidths in the tetramethyl-substituted nitroxide series has been thoroughly studied by Burks *et al.* [66], who revealed that the carbonyl double bond at 4-position in a piperidine nitroxide allows conformational diversity that results in a narrowing of the EPR line. They proposed a series of new piperidine structures with an exocyclic carbon-carbon double bond at 4-position, that retained narrow linewidths and allowed introduction of structural diversity for various applications. Unfortunately, it is likely that lipophilic tetraethyl-substituted piperidine nitroxides bearing an exocyclic double bond would also be substrates to fast P450-induced hydrogen atom abstraction in  $\alpha$ -position to the  $sp^2$  carbon of the ring, followed by destruction of the probe *in vivo*.

Absence of the carbonyl function in the tetraethyl piperidine probe TEEPOL afforded higher stability and retention of an EPR signal. However, this compound was also extensively transformed, mainly via hydroxylation and dehydrogenation of the ethyl groups, which led to evolution of the nitrogen coupling constant and of the spectral linewidth. Should hydroxylation and dehydrogenation be general transformations of tetraethyl-substituted nitroxides by P450 *in vivo*, their use as probes in studies where the hyperfine coupling constants and EPR linewidths are read-out parameters, such as pH or oximetry measurements [67,68], would be compromised. Systematic evaluation of the metabolic stability of other tetraethyl-substituted nitroxide structures is thus required.

Several strategies could be applied to circumvent the metabolic biotransformation of tetraethyl nitroxides by P450. First, reduction of the binding affinity to P450 could be obtained by decreasing the lipophilicity and adding charged functional groups, such as carboxylate or phosphate groups. Alternatively, the nitroxide probe could be covalently attached to a larger molecule to restrict access to the active site of P450, which is buried in the protein core. In a previous study, we showed that the covalent binding of cyclic nitron spin traps to a permethylated  $\beta$ -cyclodextrin moiety could prevent the degradation of corresponding superoxide-derived nitroxide spin adducts by P450 heme in RLM, while only partial protection was afforded by covalent binding to triphenylphosphonium groups [69]. Also, the encapsulation of nitroxides in supramolecular structures, such as liposomes [70], proteinaceous microspheres [71], or lipid nanocapsules [72], previously proposed to protect tetramethyl-substituted nitroxides from ascorbate-induced reduction could also be efficient to protect tetramethyl-substituted nitroxides from P450 metabolism. Caution must be taken, however, as all these strategies are likely to largely impact not only the metabolism but also the distribution and excretion of the probe *in vivo*.

## Acknowledgments:

The authors wish to thank Dr. P. Dansette for his invaluable help in HPLC-HRMS experiments and Dr. J.-L. Boucher and S. Lajnef for the preparation of RLM. They are also deeply grateful to Drs. P. Dansette, D. Mansuy, and J.-L. Boucher for stimulating discussions on P450 reactions and critical reading of the manuscript. Work by N. Babić was supported by Sorbonne University Paris Cité (international PhD contract 2015).

## Supplementary material:

Supplementary data to this article (HRMS analysis of pure TEEPONE and TEEPOL, EasySpin simulations, and DFT calculations) can be found online at <https://doi.org/10.1016/j.freeradbiomed.2020.05.021>.

## References

- [1] N. Kocherginsky, H.M. Swartz, Nitroxide Spin Labels: Reactions in Biology and Chemistry, CRC Press, 1995.
- [2] C.L. Rayner, S.E. Bottle, G.A. Gole, M.S. Ward, N.L. Barnett, Real-time quantification of oxidative stress and the protective effect of nitroxide antioxidants, *Neurochem. Int.* 92 (2016) 1–12. <https://doi.org/10.1016/j.neuint.2015.11.003>.
- [3] Z. Zhelev, V. Gadjeva, I. Aoki, R. Bakalova, T. Saga, Cell-penetrating nitroxides as molecular sensors for imaging of cancer in vivo, based on tissue redox activity, *Mol. Biosyst.* 8 (2012) 2733–2740. <https://doi.org/10.1039/c2mb25128k>.
- [4] N. Le Breton, M. Martinho, E. Mileo, E. Etienne, G. Gerbaud, B. Guigliarelli, V. Belle, Exploring intrinsically disordered proteins using site-directed spin labeling electron paramagnetic resonance spectroscopy, *Front. Mol. Biosci.* 2 (2015) 21. <https://doi.org/10.3389/fmolb.2015.00021>.
- [5] R. Ahmad, P. Kuppusamy, Theory, instrumentation, and applications of electron paramagnetic resonance oximetry, *Chem. Rev.* 110 (2010) 3212–3236. <https://doi.org/10.1021/cr900396q>.
- [6] V.V. Khramtsov, In vivo molecular electron paramagnetic resonance-based spectroscopy and imaging of tumor microenvironment and redox using functional paramagnetic probes, *Antioxid. Redox Signal.* 28 (2018) 1365–1377. <https://doi.org/10.1089/ars.2017.7329>.
- [7] M. Elas, K. Ichikawa, H.J. Halpern, Oxidative stress imaging in live animals with techniques based on electron paramagnetic resonance, *Radiat. Res.* 177 (2012) 514–523.
- [8] F.A. Villamena, Reactive species detection in biology: from fluorescence to electron paramagnetic resonance spectroscopy, Elsevier, Amsterdam ; Boston, 2017.
- [9] R.G. Hicks, ed., Stable radicals: fundamentals and applied aspects of odd-electron compounds, Wiley, The Atrium, Chichester, UK ; [Hoboken, N.J.], 2010.
- [10] M.C. Krishna, D.A. Grahame, A. Samuni, J.B. Mitchell, A. Russo, Oxoammonium cation intermediate in the nitroxide-catalyzed dismutation of superoxide., *Proc. Natl. Acad. Sci.* 89 (1992) 5537–5541. <https://doi.org/10.1073/pnas.89.12.5537>.
- [11] H.M. Swartz, Principles of the metabolism of nitroxides and their implications for spin trapping, *Free Radic. Res. Commun.* 9 (1990) 399–405.

- [12] H.M. Swartz, M. Sentjerc, P.D. Morse, Cellular metabolism of water-soluble nitroxides: Effect on rate of reduction of cell/nitroxide ratio, oxygen concentrations and permeability of nitroxides, *Biochim. Biophys. Acta BBA - Mol. Cell Res.* 888 (1986) 82–90. [https://doi.org/10.1016/0167-4889\(86\)90073-X](https://doi.org/10.1016/0167-4889(86)90073-X).
- [13] A. Iannone, H. Hu, A. Tomasi, V. Vannini, H.M. Swartz, Metabolism of aqueous soluble nitroxides in hepatocytes: effects of cell integrity, oxygen, and structure of nitroxides, *Biochim. Biophys. Acta.* 991 (1989) 90–96. [https://doi.org/10.1016/0304-4165\(89\)90033-0](https://doi.org/10.1016/0304-4165(89)90033-0).
- [14] K.-Y. Chen, M.G. McLaughlin, Differences in the reduction kinetics of incorporated spin labels in undifferentiated and differentiated mouse neuroblastoma cells, *Biochim. Biophys. Acta BBA - Mol. Cell Res.* 845 (1985) 189–195. [https://doi.org/10.1016/0167-4889\(85\)90176-4](https://doi.org/10.1016/0167-4889(85)90176-4).
- [15] A.T. Quintanilha, L. Packer, Surface localization of sites of reduction of nitroxide spin-labeled molecules in mitochondria, *Proc. Natl. Acad. Sci. U. S. A.* 74 (1977) 570–574. <https://doi.org/10.1073/pnas.74.2.570>.
- [16] K. Chen, J.F. Glockner, P.D. Morse, H.M. Swartz, Effects of oxygen on the metabolism of nitroxide spin labels in cells, *Biochemistry.* 28 (1989) 2496–2501. <https://doi.org/10.1021/bi00432a022>.
- [17] A. Ueda, S. Nagase, H. Yokoyama, M. Tada, H. Noda, H. Ohya, H. Kamada, A. Hirayama, A. Koyama, Importance of renal mitochondria in the reduction of TEMPOL, a nitroxide radical, *Mol. Cell. Biochem.* 244 (2003) 119–124.
- [18] J.F. Keana, S. Pou, G.M. Rosen, Nitroxides as potential contrast enhancing agents for MRI application: influence of structure on the rate of reduction by rat hepatocytes, whole liver homogenate, subcellular fractions, and ascorbate, *Magn. Reson. Med.* 5 (1987) 525–536.
- [19] A. Iannone, A. Tomasi, V. Vannini, H.M. Swartz, Metabolism of nitroxide spin labels in subcellular fraction of rat liver: I. Reduction by microsomes, *Biochim. Biophys. Acta BBA - Gen. Subj.* 1034 (1990) 285–289. [https://doi.org/10.1016/0304-4165\(90\)90052-X](https://doi.org/10.1016/0304-4165(90)90052-X).
- [20] Y. Samuni, J. Gamson, A. Samuni, K. Yamada, A. Russo, M.C. Krishna, J.B. Mitchell, Factors influencing nitroxide reduction and cytotoxicity in vitro, *Antioxid. Redox Signal.* 6 (2004) 587–595. <https://doi.org/10.1089/152308604773934341>.
- [21] Z. Ma, Q. Huang, J.M. Bobbitt, Oxoammonium salts. 5. A new synthesis of hindered piperidines leading to unsymmetrical TEMPO-type nitroxides. Synthesis and enantioselective oxidations with chiral nitroxides and chiral oxoammonium salts, *J. Org. Chem.* 58 (1993) 4837–4843. <https://doi.org/10.1021/jo00070a018>.
- [22] I.A. Kirilyuk, A.A. Bobko, I.A. Grigor'ev, V.V. Khramtsov, Synthesis of the tetraethyl substituted pH-sensitive nitroxides of imidazole series with enhanced stability towards reduction, *Org. Biomol. Chem.* 2 (2004) 1025–1030. <https://doi.org/10.1039/B400252K>.
- [23] K.E. Fairfull-Smith, F. Brackmann, S.E. Bottle, The Synthesis of Novel Isoindoline Nitroxides Bearing Water-Solubilising Functionality, *Eur. J. Org. Chem.* 2009 (2009) 1902–1915. <https://doi.org/10.1002/ejoc.200801255>.
- [24] Y. Kinoshita, K.-I. Yamada, T. Yamasaki, H. Sadasue, K. Sakai, H. Utsumi, Development of novel nitroxyl radicals for controlling reactivity with ascorbic acid, *Free Radic. Res.* 43 (2009) 565–571. <https://doi.org/10.1080/10715760902914575>.
- [25] K. Sakai, K. Yamada, T. Yamasaki, Y. Kinoshita, F. Mito, H. Utsumi, Effective 2,6-substitution of piperidine nitroxyl radical by carbonyl compound, *Tetrahedron.* 66 (2010) 2311–2315. <https://doi.org/10.1016/j.tet.2010.02.004>.
- [26] J.T. Paletta, M. Pink, B. Foley, S. Rajca, A. Rajca, Synthesis and reduction kinetics of sterically shielded pyrrolidine nitroxides, *Org. Lett.* 14 (2012) 5322–5325. <https://doi.org/10.1021/ol302506f>.
- [27] A. Rajca, Y. Wang, M. Boska, J.T. Paletta, A. Olankitwanit, M.A. Swanson, D.G. Mitchell, S.S. Eaton, G.R. Eaton, S. Rajca, Organic radical contrast agents for magnetic resonance imaging, *J. Am. Chem. Soc.* 134 (2012) 15724–15727. <https://doi.org/10.1021/ja3079829>.

- [28] A.P. Jagtap, I. Krstic, N.C. Kunjir, R. Hänsel, T.F. Prisner, S.T. Sigurdsson, Sterically shielded spin labels for in-cell EPR spectroscopy: analysis of stability in reducing environment, *Free Radic. Res.* 49 (2015) 78–85. <https://doi.org/10.3109/10715762.2014.979409>.
- [29] J.L. Hodgson, M. Namazian, S.E. Bottle, M.L. Coote, One-electron oxidation and reduction potentials of nitroxide antioxidants: A theoretical study, *J. Phys. Chem. A.* 111 (2007) 13595–13605. <https://doi.org/10.1021/jp074250e>.
- [30] J.P. Blinco, J.L. Hodgson, B.J. Morrow, J.R. Walker, G.D. Will, M.L. Coote, S.E. Bottle, Experimental and Theoretical Studies of the Redox Potentials of Cyclic Nitroxides, *J. Org. Chem.* 73 (2008) 6763–6771. <https://doi.org/10.1021/jo801099w>.
- [31] Y. Kinoshita, K. Yamada, T. Yamasaki, F. Mito, M. Yamato, N. Kosem, H. Deguchi, C. Shirahama, Y. Ito, K. Kitagawa, N. Okukado, K. Sakai, H. Utsumi, In vivo evaluation of novel nitroxyl radicals with reduction stability, *Free Radic. Biol. Med.* 49 (2010) 1703–1709. <https://doi.org/10.1016/j.freeradbiomed.2010.08.027>.
- [32] T. Yamasaki, F. Mito, Y. Ito, S. Pandian, Y. Kinoshita, K. Nakano, R. Murugesan, K. Sakai, H. Utsumi, K. Yamada, Structure-reactivity relationship of piperidine nitroxide: electrochemical, ESR and computational studies, *J. Org. Chem.* 76 (2011) 435–440. <https://doi.org/10.1021/jo101961m>.
- [33] T.B. Kajer, K.E. Fairfull-Smith, T. Yamasaki, K. Yamada, S. Fu, S.E. Bottle, C.L. Hawkins, M.J. Davies, Inhibition of myeloperoxidase- and neutrophil-mediated oxidant production by tetraethyl and tetramethyl nitroxides, *Free Radic. Biol. Med.* 70 (2014) 96–105. <https://doi.org/10.1016/j.freeradbiomed.2014.02.011>.
- [34] M. Emoto, F. Mito, T. Yamasaki, K.-I. Yamada, H. Sato-Akaba, H. Hirata, H. Fujii, A novel ascorbic acid-resistant nitroxide in fat emulsion is an efficient brain imaging probe for in vivo EPR imaging of mouse, *Free Radic. Res.* 45 (2011) 1325–1332. <https://doi.org/10.3109/10715762.2011.618499>.
- [35] M.C. Emoto, K.-I. Yamada, M. Yamato, H.G. Fujii, Novel ascorbic acid-resistant nitroxide in a lipid emulsion: an efficient brain imaging contrast agent for MRI of small rodents, *Neurosci. Lett.* 546 (2013) 11–15. <https://doi.org/10.1016/j.neulet.2013.04.044>.
- [36] X. Wang, M. Emoto, A. Sugimoto, Y. Miyake, K. Itto, M. Amasaka, S. Xu, H. Hirata, H. Fujii, H. Arimoto, Synthesis of <sup>15</sup>N-labeled 4-oxo-2,2,6,6-tetraethylpiperidine nitroxide for EPR brain imaging, *Tetrahedron Lett.* 55 (2014) 2146–2149. <https://doi.org/10.1016/j.tetlet.2014.02.063>.
- [37] B. Testa, S.D. Krämer, The biochemistry of drug metabolism--an introduction: part 1. Principles and overview, *Chem. Biodivers.* 3 (2006) 1053–1101. <https://doi.org/10.1002/cbdv.200690111>.
- [38] P. Kremers, P. Beaune, T. Cresteil, J. Graeve, S. Columelli, J.-P. Leroux, J.E. Gielen, Cytochrome P-450 Monooxygenase Activities in Human and Rat Liver Microsomes, *Eur. J. Biochem.* 118 (1981) 599–606. <https://doi.org/10.1111/j.1432-1033.1981.tb05561.x>.
- [39] M.M. Bradford, A rapid and sensitive method for the quantitation of microgram quantities of protein utilizing the principle of protein-dye binding, *Anal. Biochem.* 72 (1976) 248–254. [https://doi.org/10.1016/0003-2697\(76\)90527-3](https://doi.org/10.1016/0003-2697(76)90527-3).
- [40] T. Omura, R. Sato, The carbon monoxide-binding pigment of liver microsomes. II. Solubilization, purification, and properties, *J. Biol. Chem.* 239 (1964) 2379–2385.
- [41] J.L. Vermilion, M.J. Coon, Purified liver microsomal NADPH-cytochrome P-450 reductase. Spectral characterization of oxidation-reduction states, *J. Biol. Chem.* 253 (1978) 2694–2704.
- [42] S. Stoll, A. Schweiger, EasySpin, a comprehensive software package for spectral simulation and analysis in EPR, *J. Magn. Reson.* 178 (2006) 42–55. <https://doi.org/10.1016/j.jmr.2005.08.013>.
- [43] R. Lauricella, A. Allouch, V. Roubaud, J.-C. Bouteiller, B. Tuccio, A new kinetic approach to the evaluation of rate constants for the spin trapping of superoxide/hydroperoxyl radical by nitrones in aqueous media, *Org. Biomol. Chem.* 2 (2004) 1304. <https://doi.org/10.1039/b401333f>.
- [44] C.D. Smith, J.P. Bartley, S.E. Bottle, A.S. Micallef, D.A. Reid, Electrospray ionization mass spectrometry of stable nitroxide free radicals and two isoindoline nitroxide dimers, *J. Mass Spectrom.* 35 (2000) 607–611. [https://doi.org/10.1002/\(SICI\)1096-9888\(200005\)35:5<607::AID-JMS967>3.0.CO;2-7](https://doi.org/10.1002/(SICI)1096-9888(200005)35:5<607::AID-JMS967>3.0.CO;2-7).



- [45] F. Neese, The ORCA program system: The ORCA program system, Wiley Interdiscip. Rev. Comput. Mol. Sci. 2 (2012) 73–78. <https://doi.org/10.1002/wcms.81>.
- [46] A.D. Becke, A new mixing of Hartree–Fock and local density-functional theories, J. Chem. Phys. 98 (1993) 1372–1377. <https://doi.org/10.1063/1.464304>.
- [47] C. Lee, W. Yang, R.G. Parr, Development of the Colle-Salvetti correlation-energy formula into a functional of the electron density, Phys. Rev. B. 37 (1988) 785–789. <https://doi.org/10.1103/PhysRevB.37.785>.
- [48] A. Schäfer, C. Huber, R. Ahlrichs, Fully optimized contracted Gaussian basis sets of triple zeta valence quality for atoms Li to Kr, J. Chem. Phys. 100 (1994) 5829–5835. <https://doi.org/10.1063/1.467146>.
- [49] F. Neese, An improvement of the resolution of the identity approximation for the formation of the Coulomb matrix, J. Comput. Chem. 24 (2003) 1740–1747. <https://doi.org/10.1002/jcc.10318>.
- [50] F. Weigend, Accurate Coulomb-fitting basis sets for H to Rn, Phys. Chem. Chem. Phys. 8 (2006) 1057. <https://doi.org/10.1039/b515623h>.
- [51] A. Klamt, G. Schüürmann, COSMO: a new approach to dielectric screening in solvents with explicit expressions for the screening energy and its gradient, J. Chem. Soc. Perkin Trans. 2. (1993) 799–805. <https://doi.org/10.1039/P29930000799>.
- [52] D.P. Chong, ed., Recent advances in density functional methods, World Scientific, Singapore ; River Edge, N.J, 1995.
- [53] R. Improta, V. Barone, Interplay of Electronic, Environmental, and Vibrational Effects in Determining the Hyperfine Coupling Constants of Organic Free Radicals, Chem. Rev. 104 (2004) 1231–1254. <https://doi.org/10.1021/cr960085f>.
- [54] A. Iannone, A. Bini, H.M. Swartz, A. Tomasi, V. Vannini, Metabolism in Rat-Liver Microsomes of the Nitroxide Spin Probe Tempol, Biochem. Pharmacol. 38 (1989) 2581–2586. [https://doi.org/10.1016/0006-2952\(89\)90541-8](https://doi.org/10.1016/0006-2952(89)90541-8).
- [55] C. Kroll, H.-H. Borchert, Metabolism of the stable nitroxyl radical 4-oxo-2,2,6,6-tetramethylpiperidine-N-oxyl (TEMPONE), Eur. J. Pharm. Sci. 8 (1999) 5–9. [https://doi.org/10.1016/S0928-0987\(98\)00047-5](https://doi.org/10.1016/S0928-0987(98)00047-5).
- [56] T.D. Porter, The roles of cytochrome b5 in cytochrome P450 reactions, J. Biochem. Mol. Toxicol. 16 (2002) 311–316. <https://doi.org/10.1002/jbt.10052>.
- [57] W. Yin, K. Mitra, R.A. Stearns, T.A. Baillie, S. Kumar, Conversion of the 2,2,6,6-Tetramethylpiperidine Moiety to a 2,2-Dimethylpyrrolidine by Cytochrome P450: Evidence for a Mechanism Involving Nitroxide Radicals and Heme Iron, Biochemistry. 43 (2004) 5455–5466. <https://doi.org/10.1021/bi035944q>.
- [58] F.P. Guengerich, Common and Uncommon Cytochrome P450 Reactions Related to Metabolism and Chemical Toxicity, Chem. Res. Toxicol. 14 (2001) 611–650. <https://doi.org/10.1021/tx0002583>.
- [59] A. Rettie, A. Rettenmeier, W. Howald, T. Baillie, Cytochrome P-450--catalyzed formation of delta 4-VPA, a toxic metabolite of valproic acid, Science. 235 (1987) 890–893. <https://doi.org/10.1126/science.3101178>.
- [60] C.A. Reilly, W.J. Ehlhardt, D.A. Jackson, P. Kulanthaivel, A.E. Mutlib, R.J. Espina, D.E. Moody, D.J. Crouch, G.S. Yost, Metabolism of Capsaicin by Cytochrome P450 Produces Novel Dehydrogenated Metabolites and Decreases Cytotoxicity to Lung and Liver Cells, Chem. Res. Toxicol. 16 (2003) 336–349. <https://doi.org/10.1021/tx025599q>.
- [61] D.F.V. Lewis, M.N. Jacobs, M. Dickins, Compound lipophilicity for substrate binding to human P450s in drug metabolism, Drug Discov. Today. 9 (2004) 530–537. [https://doi.org/10.1016/S1359-6446\(04\)03115-0](https://doi.org/10.1016/S1359-6446(04)03115-0).
- [62] C.R. Jefcoate, Measurement of substrate and inhibitor binding to microsomal cytochrome P-450 by optical-difference spectroscopy, Methods Enzymol. 52 (1978) 258–279.
- [63] J.B. Schenkman, S.G. Sligar, D.L. Cinti, Substrate interaction with cytochrome P-450, Pharmacol. Ther. 12 (1981) 43–71.

- [64] D.J. Fort, D.A. Dawson, J.A. Bantle, Development of a metabolic activation system for the frog embryo teratogenesis assay: *Xenopus* (FETAX), *Teratog. Carcinog. Mutagen.* 8 (1988) 251–263. <https://doi.org/10.1002/tcm.1770080502>.
- [65] H.J. Renaud, J.Y. Cui, M. Khan, C.D. Klaassen, Tissue Distribution and Gender-Divergent Expression of 78 Cytochrome P450 mRNAs in Mice, *Toxicol. Sci.* 124 (2011) 261–277. <https://doi.org/10.1093/toxsci/kfr240>.
- [66] S.R. Burks, M.A. Makowsky, Z.A. Yaffe, C. Hoggie, P. Tsai, S. Muralidharan, M.K. Bowman, J.P.Y. Kao, G.M. Rosen, The effect of structure on nitroxide EPR spectral linewidth, *J. Org. Chem.* 75 (2010) 4737–4741. <https://doi.org/10.1021/jo1005747>.
- [67] A.A. Bobko, T.D. Eubank, J.L. Voorhees, O.V. Efimova, I.A. Kirilyuk, S. Petryakov, D.G. Trofimov, C.B. Marsh, J.L. Zweier, I.A. Grigor'ev, A. Samouilov, V.V. Khramtsov, In vivo monitoring of pH, redox status, and glutathione using L-band EPR for assessment of therapeutic effectiveness in solid tumors, *Magn. Reson. Med.* 67 (2012) 1827–1836. <https://doi.org/10.1002/mrm.23196>.
- [68] V.V. Khramtsov, A.A. Bobko, M. Tseytlin, B. Driesschaert, Exchange Phenomena in the Electron Paramagnetic Resonance Spectra of the Nitroxyl and Trityl Radicals: Multifunctional Spectroscopy and Imaging of Local Chemical Microenvironment, *Anal. Chem.* 89 (2017) 4758–4771. <https://doi.org/10.1021/acs.analchem.6b03796>.
- [69] N. Bézière, M. Hardy, F. Poulhès, H. Karoui, P. Tordo, O. Ouari, Y.-M. Frapart, A. Rockenbauer, J.-L. Boucher, D. Mansuy, F. Peyrot, Metabolic stability of superoxide adducts derived from newly developed cyclic nitron spin traps, *Free Radic. Biol. Med.* 67 (2014) 150–158. <https://doi.org/10.1016/j.freeradbiomed.2013.10.812>.
- [70] J.F. Glockner, H.C. Chan, H.M. Swartz, In vivo oximetry using a nitroxide-liposome system, *Magn. Reson. Med.* 20 (1991) 123–133. <https://doi.org/10.1002/mrm.1910200113>.
- [71] K.J. Liu, M.W. Grinstaff, J. Jiang, K.S. Suslick, H.M. Swartz, W. Wang, In vivo measurement of oxygen concentration using sonochemically synthesized microspheres, *Biophys. J.* 67 (1994) 896–901. [https://doi.org/10.1016/S0006-3495\(94\)80551-X](https://doi.org/10.1016/S0006-3495(94)80551-X).
- [72] J. Nel, C.M. Desmet, B. Driesschaert, P. Saulnier, L. Lemaire, B. Gallez, Preparation and evaluation of trityl-loaded lipid nanocapsules as oxygen sensors for electron paramagnetic resonance oximetry, *Int. J. Pharm.* 554 (2019) 87–92. <https://doi.org/10.1016/j.ijpharm.2018.11.007>.